Supporting Informations

Sonochemical-Assisted *In situ* Electrochemical Synthesis of Ag/α-Fe_2O_3/TiO_2 Nanoarrays to Harness Photoelectrochemical Energy from Water Splitting

Ibrahim Khan[12], *Ahsanulhaq Qurashi*[12*]

[1]Center of Research Excellence in Nanotechnology King Fahd University of Petroleum and Minerals, Dhahran, Saudi Arabia

[2]Chemistry Department, King Fahd University of Petroleum and Minerals, Dhahran, Saudi Arabia

Corresponding Author: Email : ahsanulhaq06@gmail.com; ahsanulhaq@kfupm.edu.sa
Tele:+96613860-7063

(**Summary of Content: 9** pages, 7 figures, and 1 table)

S1. Supplemental materials and methods

SI-1 Characterization

Figure S1 shows the AFM images of the photoanodes. AFM images were collected under ambient conditions on a Digital Instruments Nanoscope III microscope. Etched Si nanoprobe tips (Digital Instruments, Santa Barbara, CA) were used. These tips have spring constants of approximately 0.15 Nm-1 and are conical in shape with a cone angle of 20° and an effective radius of curvature at the tip of 10 nm. The AFM images presented here represent raw, unfiltered data collected in constant-force mode. The textural properties show variation for each sample due to deposition of Fe_2O_3 and Ag and anodization time. The TiO_2 sample show outgrowth morphology and the roughness can be clearly seen. Whereas, α-Fe_2O_3/TiO_2 heterostructure shows relatively lower roughness, which can be attributed to the deposition of α-Fe_2O_3, which partially covered the surface of titania. Additionally, the TiO2 growth is inhibited by these particles as well. [1,2] Small bright granular spots can be observed in Figure S1(c), in the case of Ag/α-Fe_2O_3/TiO_2. These bright granular regions are the possible silver NPs distributed over the catalyst.[3]

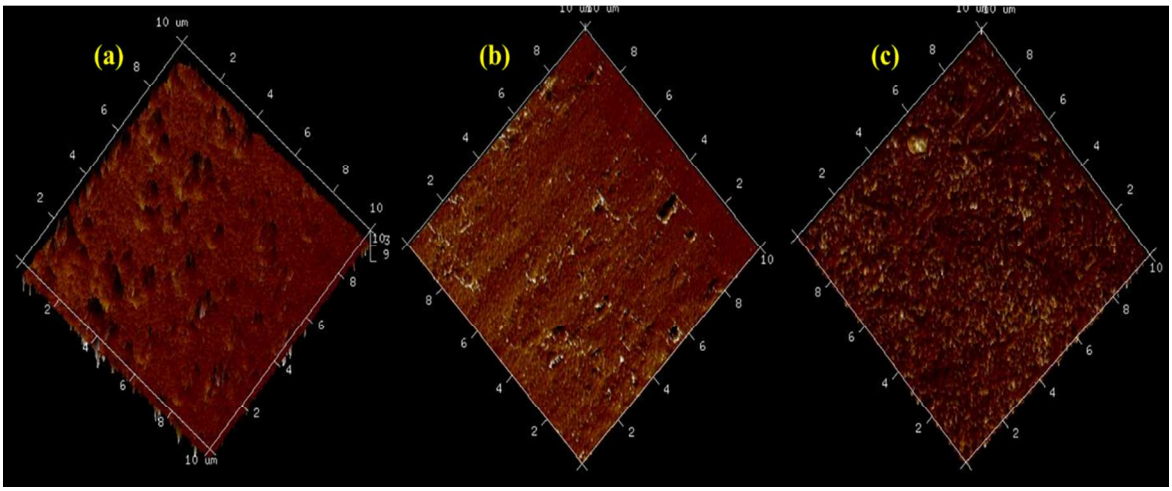

S1: Textural properties of samples via AFM (a) TiO_2 (b) α-Fe_2O_3/TiO_2 (c) Ag/α-Fe_2O_3/TiO_2

Figure S2 represents the comparative XPS profiles of the as-synthesized samples. Figure S2(a) clearly demonstrates the appearance of Ag peaks in the survey of Ag/α-Fe_2O_3/TiO_2 in the low energy region. The spectrum also showed characteristic low-intensity peaks for Fe in the higher energy regions after 700 eV. Both the regions are intentionally encircled

to identify it from the rest. The Ag peak is absent in the case of α-Fe_2O_3/TiO_2 and TiO_2. Another important observation is the intensity of the XPS spectra, which show great improvement in terms of intensity in case of Ag/α-Fe_2O_3/TiO_2 heterojunctions as compared to other samples. This phenomenon clearly demonstrated by the high-resolution spectra of Ti and O (Figure S2b and c). Additionally, there is a small shift of ~0.05-0.1 eV occurs towards higher binding energy in the XPS spectra of Ti and O. Which could be related to the successful heterojunction formation. Another important feature of the XPS profile in case of oxygen is the appearance of broad shoulder (encircled) after the incorporation of Fe, which is further intensified in the case of Ag/α-Fe_2O_3/TiO_2. This might suggest that the incorporation of Fe ions into the crystal lattice of TiO_2 influence the properties. A similar observation is reported by Abazović et al lately.[4,5]

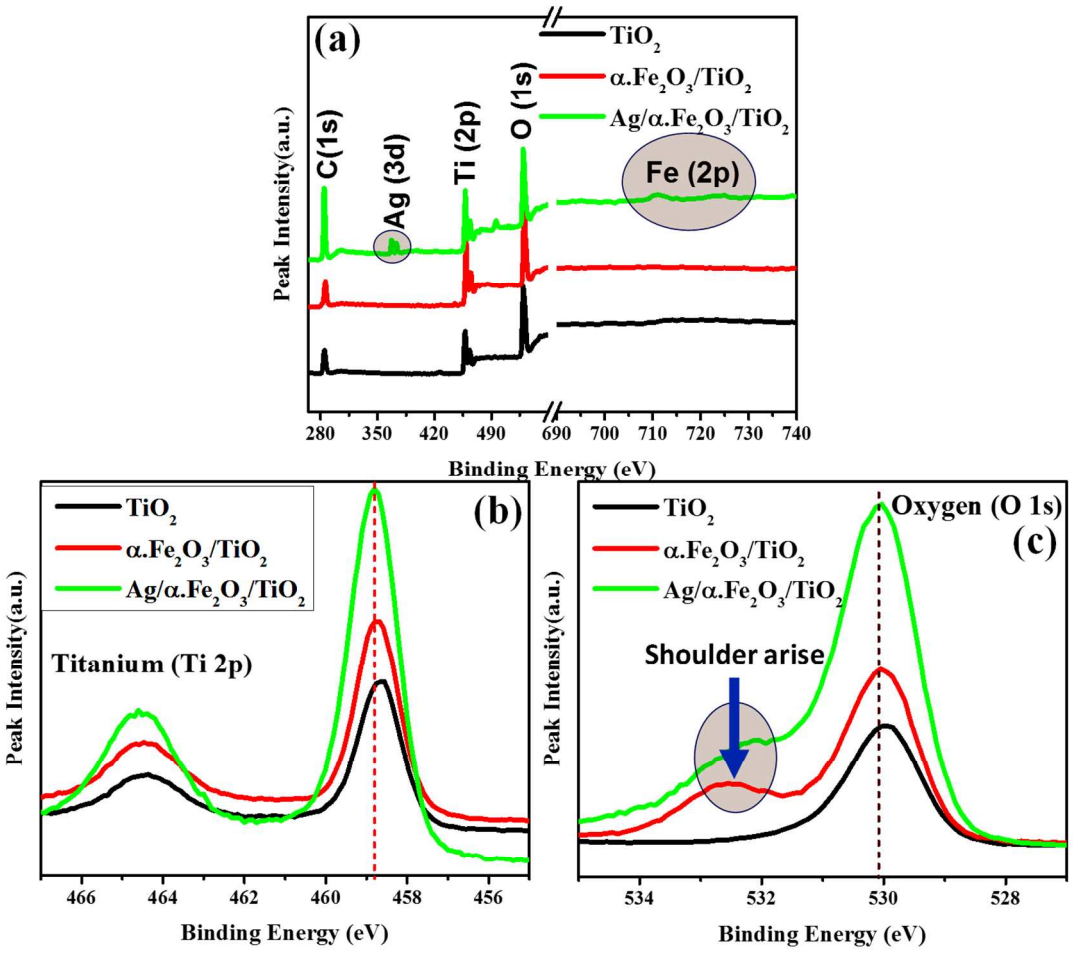

S2: (a) Comparative XPS profiles of TiO_2, α-Fe_2O_3/TiO_2 and Ag/α-Fe_2O_3/TiO_2: (a) Surveys, (b) High resolution XPS spectra of Ti (2P), and (c) O (1s).

Figure S3 showed the linear sweep voltammogram (LSV) obtained at various anodization intervals i.e. 5, 10, 20 and 30 min. It can be predicted from these results that 30 min anodization time produce sample with maximum photocurrent capacity and hence we choose 30 min anodization time for the synthesis of α.Fe_2O_3/TiO_2 and Ag/α.Fe_2O_3/TiO_2 NTAs.

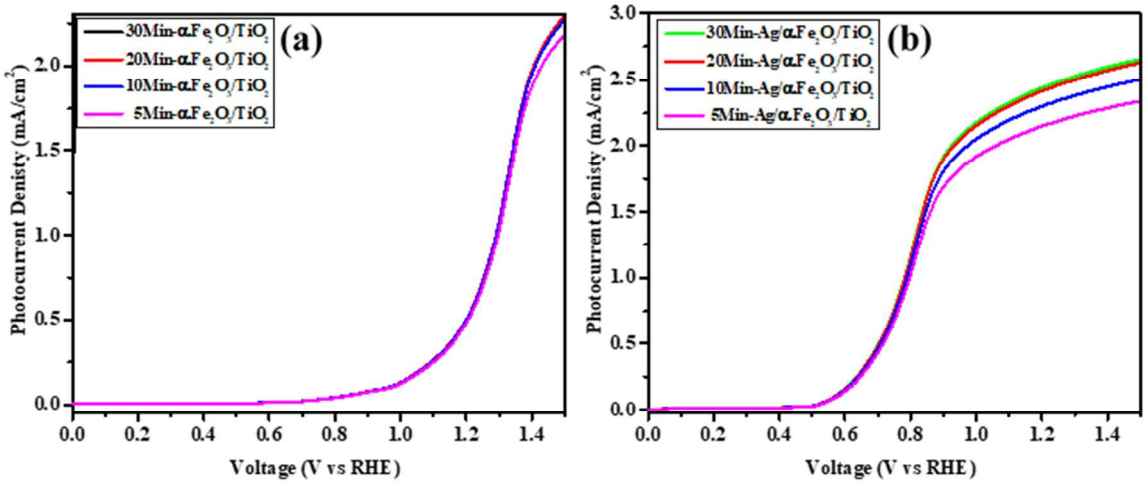

S3: (a) α.Fe_2O_3 deposition over TiO_2 NTs (b) Ag NPs deposition over α.Fe_2O_3/TiO_2 NTAs at 5, 10, 20 and 30 Mins

The chronoamperometric (*I-t*) results collected under successive light and dark cycles with ~40 s intervals further supported the results in Figure S4. The *I-t* ON/OFF cycles indicated that during light chopping, the photocurrent reached a maximum value under illumination and diminished in the dark at 1.23 V.

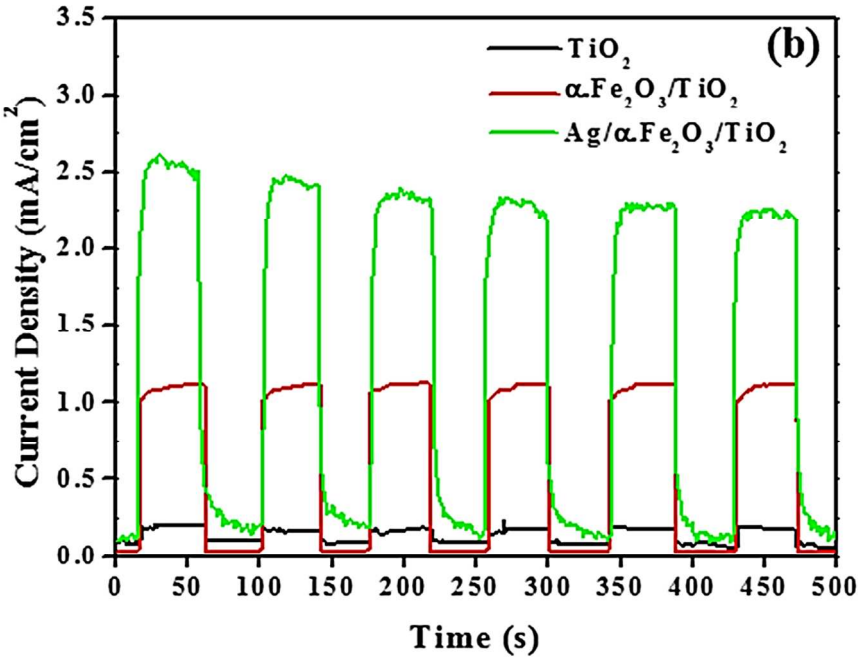

S4: Chopped visible light photocurrent density obtained at 40s/cycle for TiO_2, α-Fe_2O_3/TiO_2 and Ag/α-Fe_2O_3/TiO_2 photoanodes

Figure S5 show interfacial charge and equivalent circuit from electron impedance microscopy (EIS). In the equivalent circuit, R_S shows series resistance, C_H and R_H are Helmholtz double layer capacitance and resistance and C_{dl} and R_{dl} are the capacitance and resistance in semiconductor, respectively.[8] As suggested by the EIS results in Figure 6(d), Ag/α-Fe_2O_3/TiO_2 has the smallest radii of the semicircles compared with pristine TiO_2 and α-Fe_2O_3/TiO_2 mean the smallest resistance and charge transfer impedance. By looking to the equivalent circuit configuration, the PEC performance can be explained in terms of the total resistance value (R_T), which is the sum of R_S, R_H, and R_{dl}. The values obtained for TiO_2, α-Fe_2O_3/TiO_2 and Ag/α-Fe_2O_3/TiO_2 are 232, 115 and 65 Ωcm^{-2}, respectively. These results suggested that Ag/α-Fe_2O_3/TiO_2 possess the lowest R_t value and therefore possess lower impedance and higher charge transfer capability.

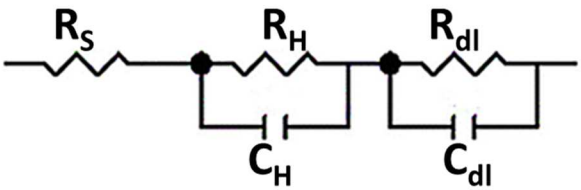

S5: Interfacial charge transfer equivalent electric circuit of Ag/α-Fe_2O_3/TiO_2 photoanodes

The % incident photon-to-current efficiency (% IPCE) and % solar to hydrogen (% STH) values obtained at 1.23 V *vs.* RHE by varying the radiation wavelength from 350 to 650 nm. Figure S6 provides the summary of the % IPCE values for TiO_2, α.Fe_2O_3/TiO_2 and Ag/α.Fe_2O_3/TiO_2 NTAs at various wavelengths. All the values are obtained under 1 SUN irradiation intensity at the incident point of the sample. The TiO_2 NTs show the higher %IPCE value of 17.13 in UV-Visible region < 400 nm. The uppermost %IPCE values of α.Fe_2O_3/TiO_2 (26.34) and Ag/α.Fe_2O_3/TiO_2 (33.84) are observed in the UV-Visible region < 400 nm, indicated that the overall efficiency of TiO_2 is significantly increased almost by two-folds. The trend continues in the visible region as well, where Ag/α.Fe_2O_3/TiO_2 showed higher %IPCE values. These results are in excellent agreement with the available literature.[9,10] The results indicated that the charge recombination is overcome with the incorporation of Fe_2O_3 and Ag, and the light absorption conversion efficiency is therefore enhanced.

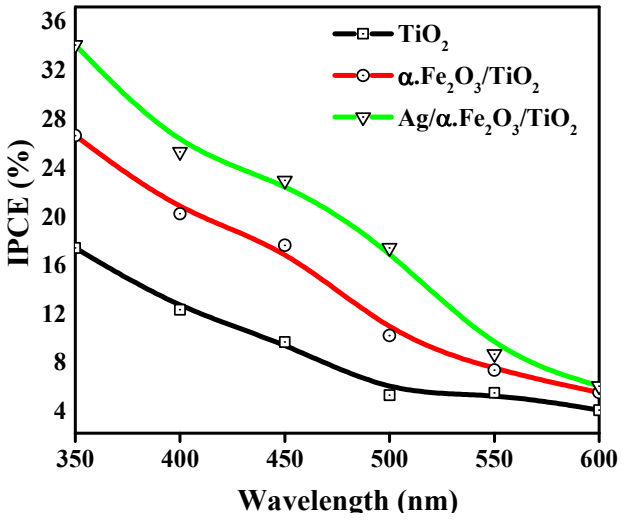

S6: %IPCE recorded for TiO_2, α-Fe_2O_3/TiO_2 and Ag/α-Fe_2O_3/TiO_2 photoanodes under 1SUN irradiations

The % STH (η) values are also recorded by using following equation.[11–13]

$$\eta = I\,(1.23 - V)/P_{light} \qquad \textbf{(i)}$$

Where I is the photocurrent density at the measurement applied bias, V is the applied bias (*vs.* RHE), and P_{light} is the incident light intensity of 100 mW cm^{-2} (AM 1.5G).

It can be observed from the table S1 that TiO2 shows higher % STH efficiency (0.94) in UV region. α.Fe_2O_3/TiO_2 and Ag/α.Fe_2O_3/TiO_2 NTAs show their highest % STH value in the visible region. Due to lower band gap and well visible light absorption capacity Ag/α.Fe_2O_3/TiO_2 NTAs show maximum %STH (2.46) at 500nm among the samples, which can be correlated with higher %IPCE value. The results are supported by the PEC water splitting measurements (Figure 6).

Table S1: % IPCE and %STH measurements at 1.23 V (vs RHE) for TiO_2, α-Fe_2O_3/TiO_2, Ag/α-Fe_2O_3/TiO_2 photoanodes at various wavelengths.

Radiations	**%STH**		
100 mW/cm^2	**TiO_2**	**α.Fe_2O_3/TiO_2**	**Ag/α.Fe_2O_3 /TiO_2**
350 nm	0.94	0.99	1.17
400 nm	0.77	1.13	1.62
450 nm	0.19	1.16	1.82
500 nm	0.17	1.04	2.46
600 nm	0.15	0.80	2.00
650 nm	0.17	0.75	1.30

SEM Images of heterostructure after measurement

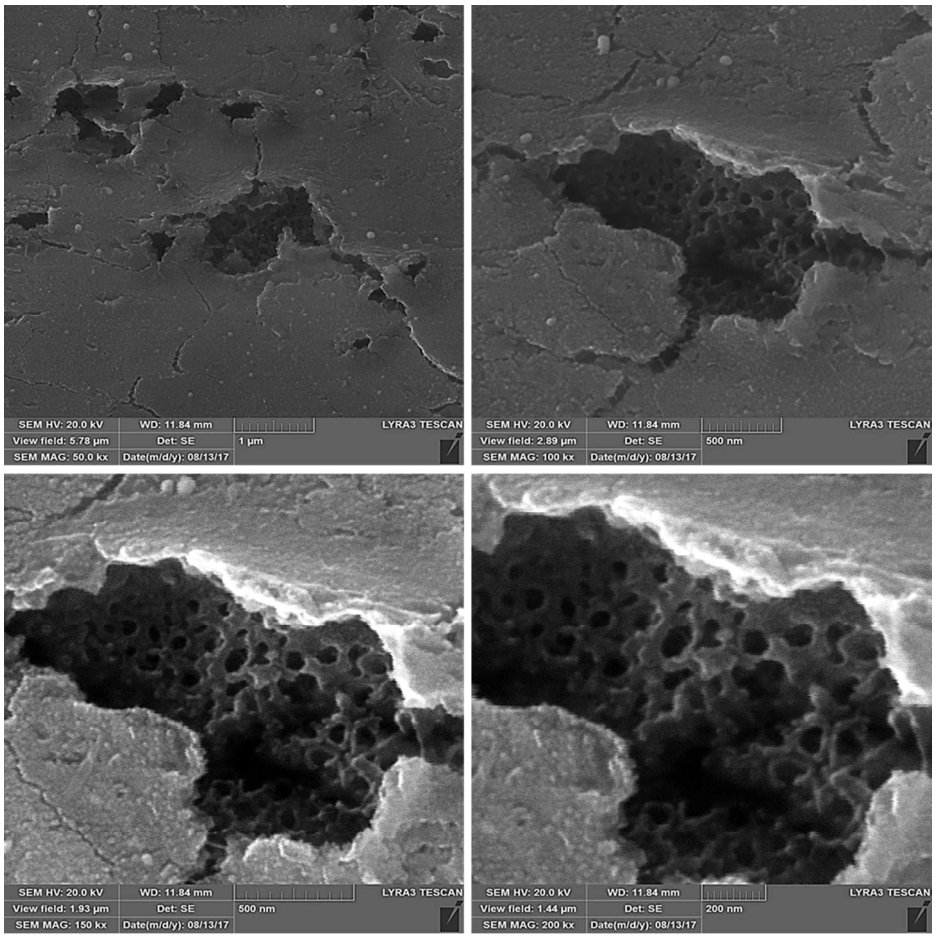

S7: Different resolution SEM images taken from Ag/α-Fe_2O_3/TiO_2 photoanodes after performing PEC water splitting measurements

References:

(1) Jiang, H.; Gao, L. Enhancing the UV inducing hydrophilicity of TiO2 thin film by doping Fe ions. *Mater. Chem. Phys.* **2003**, *77* (3), 878–881.

(2) Ismail, A. A. Synthesis and characterization of Y2O3/Fe2O3/TiO2 nanoparticles by sol–gel method. *Appl. Catal. B Environ.* **2005**, *58* (1–2), 115–121.

(3) Li, G.; Zhao, Q.; Yang, H.; Cheng, L. Antibacterial and Microstructure Properties of Titanium Surfaces Modified with Ag-Incorporated Nanotube Arrays. *Mater. Res.* **2016**, *19* (3), 735–740.

(4) Abazović, N. D.; Mirenghi, L.; Janković, I. A.; Bibić, N.; Šojić, D. V.; Abramović,

B. F.; Čomor, M. I. Synthesis and Characterization of Rutile TiO2 Nanopowders Doped with Iron Ions. *Nanoscale Res. Lett.* **2009**, *4* (6), 518–525.

(5) Beranek, R.; Kisch, H. Tuning the optical and photoelectrochemical properties of surface-modified TiO 2. *Photochem. Photobiol. Sci.* **2008**, *7* (1), 40–48.

(6) Hung, W.; Chien, T.; Tseng, C. Enhanced Photocatalytic Water Splitting by Plasmonic TiO 2 –Fe 2 O 3 Cocatalyst under Visible Light Irradiation. *J. Phys. Chem. C* **2014**, *118* (24), 12676–12681.

(7) Xu, R.; Li, H.; Zhang, W.; Yang, Z.; Liu, G.; Xu, Z.; Shao, H.; Qiao, G. The fabrication of In2O3/In2S3/Ag nanocubes for efficient photoelectrochemical water splitting. *Phys. Chem. Chem. Phys.* **2016**, *18* (4), 2710–2717.

(8) Hernández, S.; Hidalgo, D.; Sacco, A.; Chiodoni, A.; Lamberti, A.; Cauda, V.; Tresso, E.; Saracco, G. Comparison of photocatalytic and transport properties of TiO 2 and ZnO nanostructures for solar-driven water splitting. *Phys. Chem. Chem. Phys.* **2015**, *17* (12), 7775–7786.

(9) Annamalai, A.; Shinde, P. S.; Subramanian, A.; Kim, J. Y.; Kim, J. H.; Choi, S. H.; Lee, J. S.; Jang, J. S. Bifunctional TiO_2 underlayer for α-Fe_2O_3 nanorod based photoelectrochemical cells: enhanced interface and Ti^{4+} doping. *J. Mater. Chem. A* **2015**, *3* (9), 5007–5013.

(10) Chen, S.; Zeng, Q.; Bai, J.; Li, J.; Li, L.; Xia, L.; Zhou, B. Preparation of hematite with an ultrathin iron titanate layer via an in situ reaction and its stable, long-lived, and excellent photoelectrochemical performance. *Appl. Catal. B Environ.* **2017**, *218*, 690–699.

(11) Vayssieres, L. *On Solar Hydrogen and Nanotechnology*; John Wiley & Sons, 2010.

(12) Khan, I.; Ibrahim, A. A. M.; Sohail, M.; Qurashi, A. Sonochemical assisted synthesis of RGO/ZnO nanowire arrays for photoelectrochemical water splitting. *Ultrason. Sonochem.* **2017**, *37*, 669–675.

(13) Su, F.; Wang, T.; Lv, R.; Zhang, J.; Zhang, P.; Lu, J.; Gong, J. Dendritic Au/TiO2 nanorod arrays for visible-light driven photoelectrochemical water splitting. *Nanoscale* **2013**, *5* (19), 9001.